A binary beta titanium superalloy containing ordered-beta TiFe, alpha and omega

Jones, R.D.; Knowles, Sandy; Clegg, W.J.

DOI:
10.1016/j.scriptamat.2021.113905

A binary beta titanium superalloy containing ordered-beta TiFe, alpha and omega

R.D. Jones*[, a], A.J. Knowles[a, b, c], W.J. Clegg[a]

[a] *Department of Materials Science and Metallurgy, University of Cambridge, Cambridge CB3 0F3, UK*

[b] *School of Metallurgy and Materials, University of Birmingham, Birmingham B15 2TT, UK*

[c] *Department of Materials, Imperial College, South Kensington, London SW7 2AZ, UK*

**Corresponding author: robert.jones48@ntlworld.com (R.D. Jones).*

Keywords: Titanium alloys, Precipitation, Microstructure, Hardness, Metastable Phases

Abstract

Alpha-beta titanium alloys excel for aeroengine applications but are typically limited to ~550°C. An alternative strategy is reinforcement with the ordered-beta TiFe intermetallic, toward 'β-Ti superalloys', however, there has been minimal study of TiFe precipitation in the binary system.

Here, a Ti-20Fe (at.%) alloy was homogenised at 1050°C in the β-Ti phase field and aged at 600°C where the Fe supersaturation promoted TiFe precipitation. Curiously, as the TiFe volume fraction increased, the alloy hardness decreased, due to an interplay of mechanisms: (1) Fe solid solution strengthening, which reduces as the β-Ti Fe content falls to 16.2% on ageing; (2) ω precipitation strengthening, as ω-like incommensurate modulated domains were identified by transmission electron microscopy in the homogenised β-Ti parent phase and are suggested to change in size and structure after ageing, resulting in reduced ω-strengthening; (3) softening as softer TiFe and α-Ti phases precipitate from the harder ω-strengthened β-Ti parent phase.

Superalloys have excellent high temperature mechanical properties, due to their thermally stable microstructure, typically consisting of a Ni face-centred cubic (fcc) metallic matrix strengthened by coherent ordered-fcc Ni_3Al intermetallic precipitates [1,2]. Significant research has been undertaken to mimic this microstructure in other fcc systems motivated by higher melting temperatures, such as Co [3], Pt [4] and Ir [5]. Further efforts to mimic the microstructure template within body-centred cubic (bcc) systems have included: Nb [6], high-entropy alloys [7], and ferritic superalloys [8] with promising creep resistance [9,10]. The Ti-Fe system is one of few binaries able to contain β-β' phases analogous to γ-γ' Ni-based superalloys; specifically, from β bcc Ti (A2, Strukturbericht designation) to the TiFe intermetallic compound, which adopts the β' B2 ordered-bcc superlattice structure.

Various Ti-Fe phase diagrams are presented in the literature [11–14]. There is some disagreement regarding the location of certain boundaries within the phase diagram but Bo et al. [11] recently collated and reviewed the available information to re-assess the binary system. Ti has the A2 β-Ti structure above 882°C and the hexagonal α-Ti structure below 882°C. Fe stabilises the β phase. As Fe concentration increases, the β→α transformation temperature decreases. At 13.5 at.% Fe and 583°C, a eutectoid decomposition of β-Ti to α-Ti + TiFe occurs. This reaction is sluggish so β-Ti can be retained down to room temperature [15]. If a Ti-Fe alloy were homogenised close to the maximum solubility of Fe in β-Ti (~23% at 1079°C), then aged within the β-Ti + TiFe two-phase field, close to the eutectoid (β-Ti ~13.5%Fe, and TiFe ~48.9%Fe, at 583°C), the change in solubility from 23% to 13.5% Fe can be used to promote formation of TiFe precipitate-strengthened β-Ti alloys, with precipitate molar fractions (calculated by the lever rule) up to 27%.

Eutectic Ti-Fe alloys with A2 + B2 microstructures have seen some study [16–19] and can exhibit 0.2% yield strengths up to 1.8 GPa and ductility greater than 6%, in the hypereutectic

case [19]. The high strength reportedly arises from the intermetallic TiFe phase and the supersaturated β-Ti solid solution. The ductility benefits from the ultra-fine eutectic structure consisting of TiFe and the relatively soft β-Ti phase. These Ti-Fe alloys did not require any additional heat treatment after casting. Whilst eutectic alloys are promising, the controlled cooling rates required for optimum microstructure and properties imposes a limit on production routes, component size and end application. In such cases, B2 TiFe precipitate strengthening of β-Ti offers advantages, but has seen only limited study.

Van Thyne et al. [20] have conducted the most comprehensive experimental study of the Ti-Fe β phase region, considering compositions from 0-53.8 wt.% Fe and temperatures between 500°C and 1200°C. The phase diagram was deduced from a combination of metallographic studies, X-ray studies and melting range determinations. Van Thyne et al. [20] also measured the hardness of Ti-Fe alloys with 0-45% Fe, water-quenched from 1000°C, as well as with 0-15% Fe, water-quenched from 700°C. In the alloys quenched from 1000°C, the hardness peaked at 4% Fe. Van Thyne et al. [20] suggested the first peak corresponded to the composition at which β-Ti is retained upon quenching, however, the β-Ti has been retained upon quenching at much greater Fe compositions [21].

In Ti alloyed with some β stabilising elements, such as Fe or Mo, ω and/or other metastable phases can precipitate upon quenching from the β-Ti phase field [15]. The β→ω transformation occurs by a shuffle mechanism, in which atoms from neighbouring {111} planes of the bcc lattice are displaced towards one another along a <111> direction, collapsing into a single plane. This occurs with a periodicity, such that it affects two out of every three {111} planes. The ω phase can have a potent strengthening effect [22]. It has been suggested to form in a narrow concentration range, which depends upon the group number of the solute element in the periodic table and corresponds to an electron

concentration of C_e = 4.1-4.2 electrons/atom. This corresponds to a composition of ~4 wt.% Fe. Elsewhere, the ω phase has been reported to form upon ageing at 100°C to 500°C [23,24]. Upon ageing, the composition of the ω phase tends towards a pseudo-equilibrium ~4% Fe. Interestingly, this is the concentration that Van Thyne et al. [20] observed peak hardness for Ti-Fe quenched from 1000°C. Outside this narrow concentration band, in Ti-Fe alloys with a higher electron concentration, it is reported that the atom displacements associated with the phase change do not follow a fixed long-range periodicity with respect to the underlying bcc lattice [21,25,26]. As a result, ω-like nano-scale incommensurate modulated domains have recently been reported to form instead [21]. Further investigation into the precipitation strengthening of Ti-Fe alloys is required to understand the interplay between the β-Ti, B2 TiFe and metastable ω and ω-like phases.

A 40 g bar of Ti-20Fe (at.%) was prepared by vacuum arc-melting, which was turned and re-melted five times for compositional homogeneity. The bar was solution treated under vacuum at 1050 ± 5°C for 24 hours followed by water-quenching to room temperature. Ageing heat treatments were subsequently made under vacuum at 600 ± 5°C for 8, 25 and 50 hours, before water-quenching to room temperature.

The composition of the arc-melted bar was determined, in a JEOL 5800 scanning electron microscope (SEM), by large area energy dispersive X-ray spectroscopy (EDX) scans to be Ti-20.3Fe (at.%). X-ray diffraction (XRD) scans were performed on slices and ground powders of each alloy using a Bruker D8 Advance theta/theta diffractometer with position sensitive detector (LynxEye EX) using Cu-Kα radiation (λ = 1.54056 Å). The microstructure was studied in a JEOL 5800 SEM. The hardness of the alloy was measured in each of the heat-treated conditions using a Mitutoyo MVK-H2 micro-Vickers hardness testing machine with a 2 kg load and a 5 s dwell period. The mean hardness and associated error were

calculated from five hardness measurements. Electron transparent thin foils (~100 nm thick) were prepared using focussed ion beam milling and the microstructure of these alloys was studied in an FEI Tecnai F20 Field Emission Gun (FEG) Transmission Electron Microscope (TEM) and an FEI Tecnai Osiris 80-200 at 200 keV. TEM and Scanning TEM (STEM) combined with STEM-EDX were used to determine the compositions and structures of the matrix and precipitate phases.

Backscatter electron (BSE) SEM micrographs for the homogenised and 50-hour heat treated samples are shown in Fig. 1, along with respective XRD scans. After homogenisation, both SEM and XRD suggested that the Ti-Fe alloy was single phase β-Ti, with lattice parameter $a_\beta = 3.162 \pm 0.001$ Å. During the 50-hour heat treatment at 600°C, TiFe precipitated out of solution. The XRD scan confirmed the presence of the TiFe in addition to the β-Ti. The lattice parameters of the β-Ti and the TiFe were calculated as $a_\beta = 3.160 \pm 0.005$ Å and $a_{TiFe} = 2.971 \pm 0.005$ Å, giving a constrained lattice misfit of $\delta = 2(a_{TiFe} - a_\beta)/(a_{TiFe} + a_\beta) = -6.2 \pm 0.4$ %.

Further examination of the 50-hour heat treated sample by SEM (Fig. 1) identified a dark phase present between the arms of the larger TiFe precipitates, the atomic number (Z) contrast suggesting that these regions were richer in Ti than both the TiFe precipitates and the β-Ti matrix. This was attributed to the α-Ti phase, confirmed by small peaks in the XRD spectrum. Additionally, a low-angle shoulder on the bcc peak at ~58° was observed, which suggested the presence of the metastable incommensurate ω-like phase [26], motivating further TEM study.

Upon ageing, the TiFe precipitate volume fraction increased from 0 to ~20%, whilst the hardness decreased from ~550 HV to ~470 HV, see Fig. 2. The homogenised sample was

harder than ~300 HV previously reported for the β-Ti single-phase [27] and was similar to ω-strengthened β-Ti hardness, which is reported to be greater than 500 HV2.5 [24,28]. Surprisingly, the alloy softened on precipitation of TiFe, suggesting other strengthening mechanism(s) may be dominant.

There are a number of contributions to the age softening. The reduction in Fe solid solution strengthening may outweigh the increase in TiFe precipitation strengthening, as the alloy is aged. The β-Ti lattice parameter is 3.283 Å [29], whilst that for bcc Fe is 2.8604 Å [30]. This 14% size difference results in a large solid solution strengthening effect – reported to increase the yield strength by 54 MPa per at.% Fe solute [31]. The distance between the TiFe precipitates in the aged samples was relatively large, $L \approx 4$ μm, see Fig. 1b; therefore, dislocations may have been able to bypass the precipitates by Orowan bowing. The Orowan bowing stress can be calculated by:

$$\tau = \frac{\mu b}{L} \quad (1)$$

where μ is the shear modulus, b is the Burgers vector and L is the interparticle spacing. Taking, $L \approx 4$ μm, $\mu = 40$ GPa and $b = 2.74$ Å, the Orowan bowing stress was estimated as $\tau = 2.7$ MPa; therefore, the TiFe precipitate strengthening is likely to be small compared to the solid solution strengthening.

The homogenised sample and 50-hour aged sample were studied by TEM. No additional phases were observed under standard imaging conditions in the homogenised sample; however, the selected area diffraction pattern (SADP) down the {110} zone axis identified the ω phase present in both the homogenised (Fig. 3a) and aged samples (Fig. 3b). Previous studies have found that this phase often has a high volume fraction with precipitate sizes of

~2-10 nm [21,25,26,28,32,33] resulting in a large strengthening effect, sometimes even leading to embrittlement.

The commensurate athermal ω phase (Fig. 3c) is distinguishable from the incommensurate ω phase (Fig. 3d) by the position of the reflections at *HKL* + *hhh*, where *HKL* are the reflections present in the β phase and $h = 2/3$ for commensurate ω and $h > 2/3$ for the incommensurate phase [25]. The incommensurate reflections also tend to be more smeared and diffuse than the commensurate reflections. Here, the incommensurate phase was present in both conditions, demonstrated by additional reflections at $h = 0.78$ in the homogenised sample and $h = 0.74$ in the aged sample – the differing h indicating a slight change in the structure or constraint of ω between the two conditions. The formation of the incommensurate ω-like phase rather than the commensurate ω phase was expected because of the high electron concentration per atom [25]. Based upon EDX measurements of the β-Ti composition, the electron concentration per atom of the β-Ti phase after homogenisation was 4.8 (Ti-20.3Fe) and after ageing was 4.6 (Ti-16.2Fe). The corresponding Δh (where, $\Delta h = h - 0.67$) values for the additional SADP reflections were measured as 0.11 for the homogenised and 0.07 for the aged, consistent with previous studies of Ti-Fe alloys [25].

The ω phase has previously been found to be unstable at the homogenisation temperature [26] and in both conditions here, ω appears to have formed on cooling. Furthermore, recent Ti-Fe work has found the nano-scale incommensurate modulated domains are distinct from the shuffle mechanism involved in the formation of the ω phase present in Ti-Mo [21], warranting further work to determine the formation mechanism of the ω-like incommensurate phase in Ti-Fe.

STEM imaging revealed a three-phase microstructure in the 50-hour aged sample, Fig. 4. STEM-EDX maps and SADPs of each phase are also shown in Fig. 4. The composition of the β-Ti phase, point 1, was measured as 16.2 at.% Fe, slightly greater than predicted by previous thermodynamic assessments (~14%) at the eutectoid [11,13]; however, within the measurement error, ~2% [26], this agreed with the eutectoid composition quoted by Murray [13], ~15%. The SADP of point 2 confirmed that this phase was B2 TiFe by the presence of the {100} superlattice reflections and showed a cube-cube orientation relationship between the B2 TiFe and the A2 β-Ti, i.e. $[100]_{A2}//[100]_{B2}$. The composition of the TiFe (49.5% Fe) was slightly more Ti-rich than a 1:1 Ti:Fe stoichiometric composition, in agreement with previous thermodynamic assessments [11,13]. The SADP of the darker phase between the arms of the TiFe precipitates, point 3, confirmed this was α-Ti. The α phase had little Fe solubility (0.3%), as expected from literature [11–14].

The α-Ti between the arms of TiFe precipitates has not previously been studied in detail. The presence of α-Ti at 600 ± 5°C indicates that the eutectoid temperature may be higher than previous reports of 575-600°C [11]. The only experimental data taken in this region of the phase diagram appears to be that of Van Thyne et al. [20]. Due to the fine size of the α-Ti regions, it would have been challenging for Van Thyne et al. [20] to observe these regions by optical microscopy. The ω-strengthened β-Ti matrix was retained away from the primary TiFe, and the α-Ti only formed adjacent to the TiFe precipitates, corresponding to previous observations that the eutectoid decomposition is sluggish [15].

The presence of these additional α and incommensurate phases, revealed by TEM, may explain why the Ti-Fe alloy softens upon ageing. Whilst ω-strengthened β-Ti is known to be very hard (>500 HV2.5 [24,28]), the B2 TiFe intermetallic is reportedly softer, with a microhardness of ~350 HV0.5 [34]. α-Ti with 0.3 at.% Fe is also soft, with a yield strength of

~300 MPa [35], corresponding to a hardness of ~100 HV. Therefore, the precipitating TiFe and α-Ti phases may be softer than the solid-solution and ω-strengthened β-Ti parent phase. Furthermore, Dyakonova et al. [32] previously reported ω particle size to be dependent upon the electron concentration of the β-Ti matrix. Here, this would correspond to an 11 nm ω particles in the homogenised condition (C_e = 4.8) and 2 nm ω particles in the aged condition (C_e = 4.6). The ω interparticle spacing has previously been observed to be ~10 nm [32], and, based on calculations in Appendix 1 (detailed further in [36]), dislocations are likely to cut the strengthening precipitates rather than bow around them at these length scales. So if the ω particles are smaller in the aged condition, then the ω-strengthening effect would be weaker, explaining the apparent softening.

A Ti-20Fe alloy has been produced and studied in homogenised and aged conditions. Whilst the homogenised condition initially appeared to be single phase β–Ti, XRD and TEM SADPs reflections identified the presence of a metastable incommensurate phase presumed to form on cooling, which strongly contributed, alongside solid solution strengthen, to the high hardness, ~550 HV.

Following a 600 ± 5°C ageing heat treatment, selected to promote TiFe precipitation strengthening, the hardness of the alloy decreased to ~470 HV. Whilst B2 TiFe precipitation was observed, this was accompanied by simultaneous precipitation of α-Ti. In addition, the incommensurate phase was also present in the aged condition. It is suggested that the decrease in hardness is due to a combination of: a reduction in solid solution strengthening; a change in the ω structure and size; and the precipitation of TiFe and α-Ti phases, which are softer than the ω-strengthened β–Ti parent phase. Further investigation to definitively separate the interplay between these mechanisms is the basis of future work.

Acknowledgements

N Jones and R Thompson assisted with alloy production. J Barnard assisted with TEM. M Vickers and A Moss assisted with XRD. G Rought Whitta and E McGregor assisted with preliminary investigations. This work was supported by EPSRC (EP/N509486/1, EP/H022309/1, EP/H500375/1 and EP/M005607/1). A.J. Knowles was supported by UKRI Future Leaders Fellowship and Royal Academy of Engineering Research Fellowship.

References

[1] M.J. Donachie, S.J. Donachie, Superalloys: A Technical Guide, 2nd ed., ASM Int., 2002.

[2] R.C. Reed, The Superalloys: Fundamentals and Applications, 2006.

[3] H.Y. Yan, V.A. Vorontsov, J. Coakley, N.G. Jones, H.J. Stone, D. Dye, Superalloys 2012 12th Int. Symp. Superalloys (2012) 705–714.

[4] L.A. Cornish, B. Fischer, R. Völkl, MRS Bull. (2003) 632–638.

[5] Y. Yamabe-Mitarai, Y. Ro, H. Harada, T. Maruko, Metall. Mater. Trans. A 29 (1998) 537–549.

[6] G. Ghosh, G.B. Olson, Acta Mater. 55 (2007) 3281–3303.

[7] V. Soni, O.N. Senkov, B. Gwalani, D.B. Miracle, R. Banerjee, Sci. Rep. 8 (2018) 1–10.

[8] S. Naka, T. Khan, J. Phase Equilibria 18 (1997) 635–649.

[9] N.Q. Vo, C.H. Liebscher, M.J.S. Rawlings, M. Asta, D.C. Dunand, Acta Mater. 71 (2014) 89–99.

[10] C.H. Liebscher, V. Radmilovic, U. Dahmen, M. Asta, G. Ghosh, J. Mater. Sci. 48 (2013) 2067–2075.

[11] H. Bo, J. Wang, L. Duarte, C. Leinenbach, L. Liu, H. Liu, Z. Jin, Trans. Nonferrous Met. Soc. China 22 (2012) 2204–2211.

[12] L.F.S. Dumitrescu, M. Hillert, N. Saunders, J. Phase Equilibria 19 (1998) 441–448.

[13] J.L. Murray, Bull. Alloy Phase Diagrams 2 (1981) 320–334.

[14] K.C. Hari Kumar, L. Dumitrescu, B. Sundman, P. Wollants, in: Proc. Calphad XXVIII Conf., 1999.

[15] I.P. Polmear, Light Alloys - From Traditional Alloys to Nanocrystals, 2006.

[16] J. Das, K.B. Kim, F. Baier, W. Löser, A. Gebert, J. Eckert, J. Alloys Compd. 434–435 (2007) 28–31.

[17] L.C. Zhang, J. Das, H.B. Lu, C. Duhamel, M. Calin, J. Eckert, Scr. Mater. 57 (2007) 101–104.

[18] C.H. Lee, J.T. Kim, S.H. Hong, G.A. Song, J.H. Jo, S.C. Moon, K.B. Kim, Met. Mater. Int. 20 (2014) 417–421.

[19] D. V. Louzguine-Luzgin, L. V. Louzguina-Luzgina, H. Kato, A. Inoue, Mater. Reasearch Soc. Symp. Proc. 851 (2005) NN5.13.

[20] R.J. Van Thyne, H.D. Kessler, M. Hansen, Trans. Am. Soc. Met. 44 (1952) 974–989.

[21] Y. Zheng, D. Huber, H.L. Fraser, Scr. Mater. 154 (2018) 220–224.

[22] F.H. Froes, Titanium: Physical Metallurgy, Processing, and Applications, 2015.

[23] B.S. Hickman, Trans. Metall. Soc. AIME 245 (1969) 1329–1335.

[24] N.A. Vanderpuye, A.P. Miodownik, in: Sci. Technol. Appl. Titan., 1970, pp. 719–730.

[25] G.I. Nosova, N.B. D'Yakonova, I. V. Lyasotskii, Met. Sci. Heat Treat. 48 (2006) 427–

432.

[26] A.J. Knowles, N.G. Jones, O.M.D.M. Messé, J.S. Barnard, C.N. Jones, H.J. Stone, Int. J. Refract. Met. Hard Mater. 60 (2016) 160–168.

[27] P. Manda, U. Chakkingal, A.K. Singh, Mater. Charact. 96 (2014) 151–157.

[28] B.S. Hickman, J. Mater. Sci. 4 (1969) 554–563.

[29] B.W. Levinger, J. Met. 5 (1953) 195.

[30] Z.S. Basinski, W. Hume-Rothery, A.L. Sutton, Proc. R. Soc. A Math. Phys. Eng. Sci. 229 (1955) 459–467.

[31] G. Welsch, R. Boyer, E.W. Collings, Materials Properties Handbook: Titanium Alloys, 1993.

[32] N.B. Dyakonova, I. V. Lyasotsky, G.I. Nosova, Rev. Adv. Mater. Sci. 18 (2008) 703–710.

[33] I. V. Lyasotskiy, N.B. D'Yakonova, Phys. Met. Metallogr. 53 (1982) 104–111.

[34] R. Scholl, D.J. Larson, E.J. Freise, J. Appl. Phys. 39 (1968) 2186–2191.

[35] M.J. Donachie Jr., Titanium, 2000.

[36] R.D. Jones, Deformation in A2/B2 Alloys, University of Cambridge, 2016.

[37] E. Nembach, Particle Strengthening of Metals and Alloys, 1997.

Appendix 1

The unexpected drop in hardness upon ageing may relate to the size of the ω particles. Dyakonova et al [32] calculated the size of incommensurate ω particles in Ti-Fe alloys from the width of XRD peaks, for a range of different Fe concentrations, Fig. A1.

The relationship between the critical resolved shear stress and particle size is shown in Fig. A2. Dislocations can either cut the strengthening precipitates or bow around them. Smaller, finely spaced precipitates are easier for dislocations to cut, whereas it is easier for dislocations to bow around a larger, coarse distribution of precipitates. Previous observations of the ω phase in β-Ti, suggest that the interparticle spacing, L, is approximately equal to 10 nm [32]. Therefore taking, $L \approx 10$ nm, the shear modulus as $\mu = 40$ GPa and the Burgers vector as $b = 2.74$ Å, the Orowan bowing stress, Equation 1, was estimated as $\tau = 1.1$ GPa.

The particle cutting stress was estimated by considering the stress required to overcome lattice mismatch strengthening [37]

$$\tau = \frac{\left(\mu|\delta|\right)^{3/2}\left(rfb\right)^{1/2}}{\left(2S\right)^{1/2}} \qquad \text{(A1)}$$

where δ is the lattice mismatch, f is the particle volume fraction and S is the dislocation line tension. Taking, $\delta \approx 1\%$, $r = 10$ nm, $f = 0.5$ [33] and $S = \frac{1}{2}\mu b^2$, the cutting stress was:

$$\tau = \mu\left(\frac{rf}{b}\right)^{1/2}|\delta|^{3/2} = 170 \text{ MPa} \qquad \text{(A2)}$$

This suggests that dislocations cut through the ω particles rather than bow around them and therefore the critical resolved shear stress should be proportional to $r^{1/2}$, as shown in Fig. A2.

The lattice mismatch could be as high as 3.5% before the stress required to overcome the lattice mismatch strengthening is greater than the stress required for Orowan bowing.

The observed variation in hardness could therefore be described in terms of ω precipitate strengthening. In the homogenised condition, the ω particles are relatively large, r_ω = 11 nm. After ageing, the Fe content in the β-Ti matrix decreases and the ω particle size also decreases, r_ω = 2 nm. Therefore, after ageing the smaller ω particles provide less resistance to cutting. This may explain the drop in hardness that was seen in Fig. 2.

The hardness results of Van Thyne et al. [20], Fig. A1, can be reconsidered in light of the fact that the ω phase is present in both the homogenised and aged conditions and may provide the primary strengthening. The equilibrium composition of commensurate athermal ω is ~4% Fe [23,24], which corresponds to an electron concentration per atom of ~4.16. The ω peak in the SADP is sharp [25] and this corresponds to a relatively large particle size ~6 nm [32]. The formation of this commensurate ω leads to the first peak in hardness. As the Fe concentration is increased further, ω becomes incommensurate, the peaks in the SADP become more diffuse [25] and the ω particle size decreases to ~2 nm [32]. These smaller particles are easier for dislocations to cut [37] and therefore a reduction in the hardness is seen, Fig. A1. Further increase in the Fe concentration, causes the ω peaks in the SADP to become sharper [25], indicating an increase in the particle size up to ~11 nm [32]. This larger particle size would increase the hardness as the Fe concentration approaches the limit of solid solubility in β-Ti, as seen in Van Thyne's work [20]. There appears to be a good correlation between the Ti-Fe hardness results [20] and the ω particle size, calculated from XRD [32]. This supports the hypothesis that the ω phase significantly contributes towards the strengthening in these alloys and is consistent with a particle cutting mechanism.

Figures and Captions

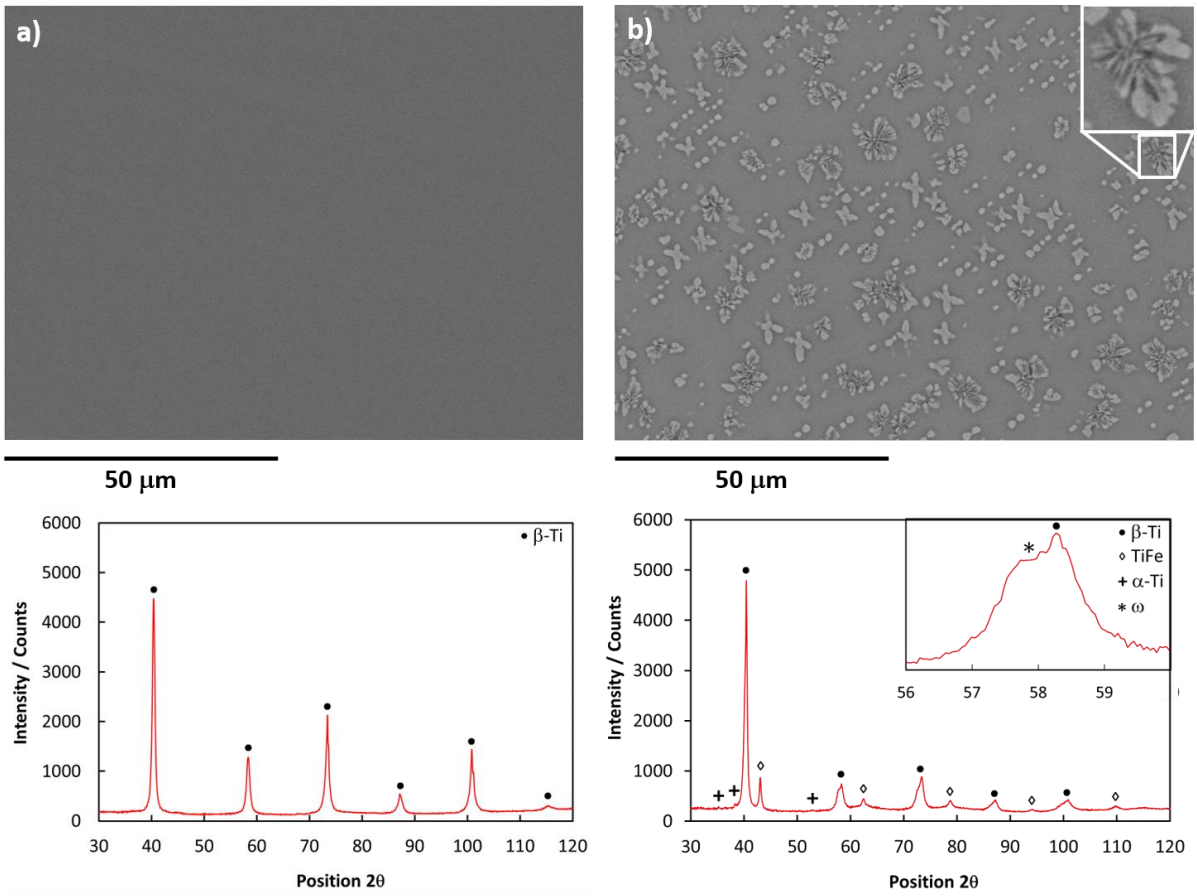

Figure 1

BSE SEM images and XRD scans for: a) homogenised sample; b) sample heat treated for 50 hours at 600°C.

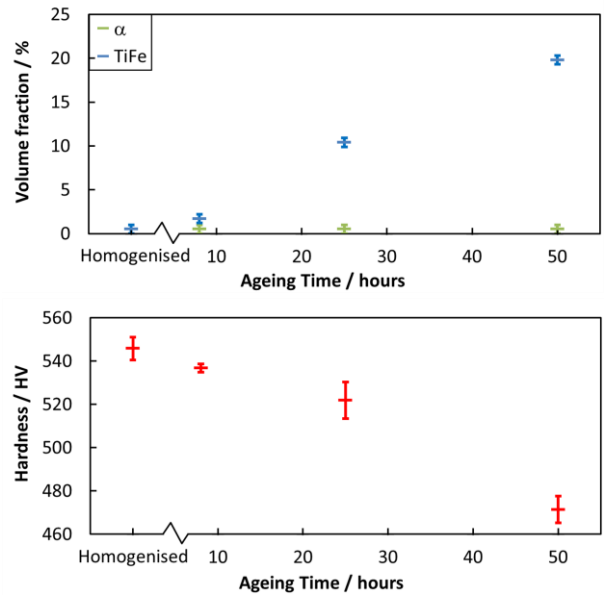

Figure 2

α and TiFe volume fraction (determined by powder XRD) and microhardness as a function of ageing time at 600°C (as homogenised and following ageing for 8, 25 and 50 hours). The hardness error bars show the standard error.

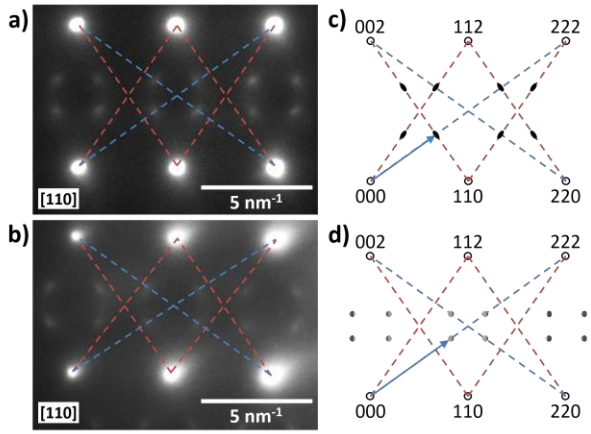

Figure 3

Ti-20Fe SADP down a {110} A2 zone axis in the: a) homogenised sample; b) 50-hour aged sample. Typical diffraction patterns for: c) the commensurate ω phase ($h = 2/3$); d) the incommensurate phase ($h > 2/3$). The black circles are reflections also present in the reciprocal bcc lattice; the arrows ([*hhh*] vectors) point towards the positions of ω-reflections, which tend to be smeared and more diffuse in the incommensurate phase – adapted from Nosova et al. [25]. The position and diffuse appearance of the reflections in the homogenised ($h = 0.78$) and the aged ($h = 0.74$) Ti-20Fe SADP indicates that the incommensurate phase is present in both conditions.

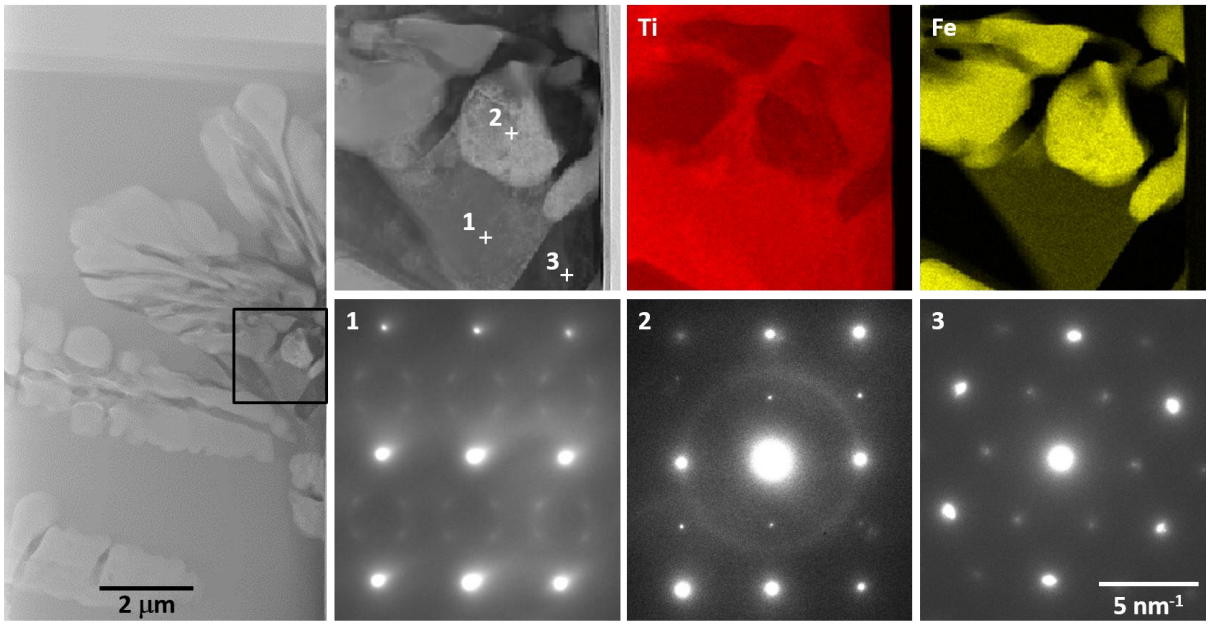

Figure 4

High-angle annular dark-field (HAADF)-STEM image of the sample heat treated for 50 hours at 600°C, with Ti and Fe EDX maps of a small area and SADP of each phase: 1) β-Ti + ω, down a [110] β-Ti zone axis; 2) TiFe, down a [110] TiFe zone axis; 3) α-Ti, down a [001] α–Ti zone axis.

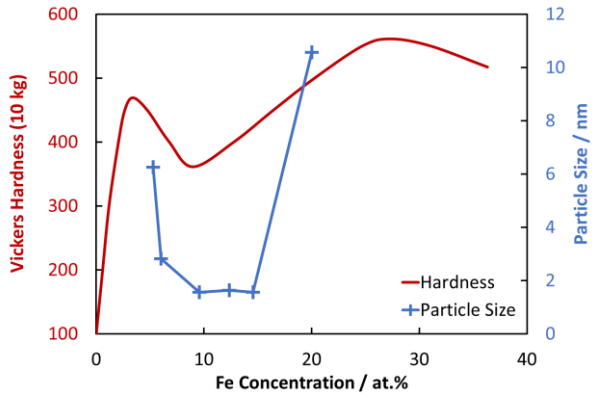

Figure A1

Vickers hardness of Ti quenched from 1000°C, data adapted from [20], and ω particle size plotted against Fe concentration, data adapted from [32].

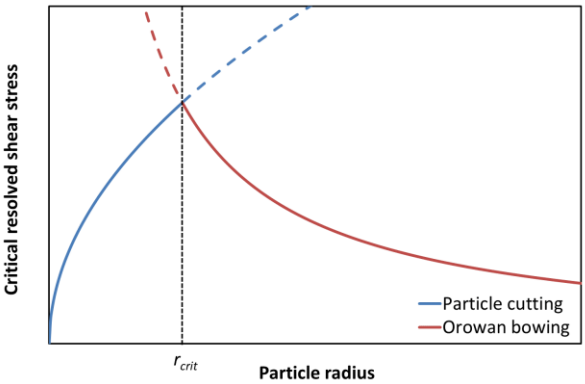

Figure A2

Critical resolved shear stress due to particle strengthening as a function of particle radius, calculated according to [37]. The stress required to cut a particle shows an $r^{1/2}$ dependence on particle size, whilst the stress required to bow around a particle shows a 1/r dependence, for a constant particle volume fraction.